

AD A9 50 112

LEVEL

①

DTIC
ELECTE
S DEC 13 1980

LOCKHEED

MISSILES & SPACE COMPANY, INC. • SUNNYVALE, CALIFORNIA

MSD
38
Pac Coa

~~CONFIDENTIAL~~

DECLASSIFIED

DECLASSIFIED

MSD-2630

LMSC LIBRARY INVENTORY - SUNNYVALE
Return to LMSC Library. Do not destroy
or transmit to another person or office.

1

LMSD LIBRARY PROPERTY
SUBSTITUTION

Borrower is responsible for safekeeping of this item and for its return to LMSC Library within loan period. If this item is not returned, borrower must provide replacement copy or reimburse LMSC Library.

AN INVESTIGATION OF THE JETEVA TOR AS A MEANS OF THRUST VECTOR CONTROL

Classified by DD254
Subject to GDS of EO 11652
Automatically Downgraded at
Two Year Intervals
Declassified on December 31 64

DOWNGRADED AT 3 YEAR INTERVALS;
DECLASSIFIED AFTER 12 YEARS.
DOD DIR 5200.10
by

S. S. EDWARDS and G. H. PARKER

"This document has been ~~CONFIDENTIAL~~ (declassified).
The internal pages still bear the former classification
markings. Reproduction in whole or in part, partial or
complete inclusion in another document, or transmittal
to another facility is prohibited unless total regrade
action is applied to all pages by Document Control."

SELL
S
DEC 18 1980
C

FEBRUARY 1958

Lockheed

DISTRIBUTION STATEMENT A
Approved for public release;
Distribution Unlimited

MISSILES and SPACE DIVISION
LOCKHEED AIRCRAFT CORPORATION - SUNNYVALE, CALIF.

DECLASSIFIED

~~CONFIDENTIAL~~ DECLASSIFIED

DECLASSIFIED
~~CONFIDENTIAL~~

LMSD-2630

COPY NO. 4
OF COPIES
SERIES _____
_____ SHEETS

DOMESTIC ORIGINALS:
DEC. 1958
DOE-VT-2630

AN INVESTIGATION OF THE JETEVATOR
AS A MEANS OF THRUST VECTOR CONTROL,

by

S. S. EDWARDS and G. H. PARKER

FEBRUARY 1958

This document contains information affecting the national defense of the United States within the meaning of the Espionage Laws, Title 18, U. S. C., Sec. 793 and 794. Its transmission or the revelation of its contents in any manner to an unauthorized person is prohibited by law.

DECLASSIFIED
~~CONFIDENTIAL~~

LOCKHEED AIRCRAFT CORPORATION

DISTRIBUTION STATEMENT A

Approved for public release;
Distribution Unlimited

MISSILES and SPACE DIVISION

210700 80 12 18 023

~~CONFIDENTIAL~~ **DECLASSIFIED**
~~CONFIDENTIAL~~

USO-2620

FOREWORD

The authors wish to acknowledge the early work done on this problem at the Naval Air Missile Test Center, Point Mugu, California, by W.A. Fiedler, inventor of the jetevator, and to thank Clinton Sherburne for his able assistance in the experimental phase of the study.

This study was presented at the Fourth U.S. Navy Symposium on Aeroballistics in November, 1957, under the title "An Analytical and Experimental Investigation of a Method of Thrust Vector Control for Solid Rocket Motors".

Accession For	
NTIS GRA&I	<input checked="" type="checkbox"/>
DTIC TAB	<input type="checkbox"/>
Unannounced	<input type="checkbox"/>
Justification	<i>Per F608</i>
<i>On file</i>	
By	
Distribution/	
Availability Codes	
Dist	Avail and/or Special
<i>A</i>	
UNANNOUNCED	

~~CONFIDENTIAL~~ **DECLASSIFIED**
~~CONFIDENTIAL~~

~~CONFIDENTIAL~~ DECLASSIFIED

TABLE OF CONTENTS

Foreword	ii
List of Figures	iv
Summary	v
Introduction	1
Symbols	3
Analysis	4
Experimental Results	25
Conclusions	36
References	37

~~CONFIDENTIAL~~ DECLASSIFIED

~~SECRET~~ DECLASSIFIED

FIGURES

Figure No.		Page
1	Jetevator Assembly	2
2	Orientation of Jetevator in Cartesian Coordinate System and Spherical Coordinate System	5
3	Criteria for Establishing Strength of Shock Due to Flow Separation	14
4	Model for the Analysis of Separated Flow Case	15
5	Schematic of Separated Flow Case with Definitions	15
6	"Cold Flow" Jetevator Test Setup	26
7	Schematic of "Cold Flow" Jetevator Test Setup	27
8	Comparison of Predicted Pressure Distribution with Experimental Data	30
9	Radial Distribution of Peak Pressures for Separated Flow Case	31
10	Comparison of Loads Predicted by Analytical Study to Experimental Data	31
11	Effect of Jetevator Hinge Location on the Pressure Distribution along Nozzle and Jetevator Centerline	33
12	Effect of Gap on Pressure Distribution along Nozzle and Jetevator Centerline.	34

~~SECRET~~ DECLASSIFIED

~~CONFIDENTIAL~~ DECLASSIFIED

SUMMARY

The jetevator is designed to control the thrust vector of solid propellant rocket engines. The device is a semi-spherical shell hinged to the rocket nozzle and rotated, at the command of a sensing unit, into the exhaust flow to produce a control force. Optimum design of the system requires maximum effectiveness with a minimum reduction in thrust.

This paper presents an analytical study of jetevators which includes analysis of control effectiveness, thrust decrement, and aerodynamic hinge moments for two flow conditions--unseparated flow in the rocket nozzle and separated flow in the nozzle due to the deflected jetevator. The factors affecting jetevator performance are discussed, and the results of experimental investigation of these factors are presented and compared with predicted results.

~~CONFIDENTIAL~~ DECLASSIFIED

INTRODUCTION

It has become increasingly apparent that, for ballistic missiles, solid propellant rocket engines have a number of logistic advantages over those powered with liquid propellants. To capitalize upon these advantages, however, the problem of stabilizing the missile by means of thrust vector control must be solved. Thrust control in the liquid engine generally is accomplished by gimbaling the rocket engines. A similar scheme for the solid propellant engine does not seem practical at the present time; consequently, other means of controlling the thrust vector must be used (Ref. 1). One method for accomplishing this is with jet vanes or aerodynamic surfaces that are immersed in the rocket exhaust stream and which are actuated to deflect the rocket thrust. A seemingly more attractive method for thrust vector control is with a device called the jetevator - a spherical ring hinged to the rocket motor exhaust nozzle free to swing in and out of the exhaust stream in response to a control servo (see Ref. 2). A photograph of jetevators installed on the four nozzles of a solid propellant engine is shown in Fig. 1.

Several advantages for jetevator control can be cited. First, for conditions in which no control is required, the jetevator is retracted from the exhaust flow. As a result, neither degradation of thrust nor thermal erosion of the jetevator materials occurs. Secondly, hinge moments and the moment of inertia can be held to low values by utilizing jetevators of spherical curvature.

Two problems exist in the development of jetevators. First, the obvious difficulty of obtaining material that will withstand the extreme heat. Secondly, the problem of the aerodynamic design with the objective of arriving at configurations having maximum effectiveness with compatible values of associated thrust decrement. This paper is concerned, primarily, with the second of these two problems.

~~CONFIDENTIAL~~ DECLASSIFIED

~~CONFIDENTIAL~~ DECLASSIFIED

LMSD-2630



Fig. 1 Jetevator Assembly

2

LOCKHEED AIRCRAFT CORPORATION

~~CONFIDENTIAL~~ DECLASSIFIED

MISSILES and SPACE DIVISION

~~CONFIDENTIAL~~ DECLASSIFIED

SYMBOLS

- A, B Coefficients of linear terms in powers series expansion
- C_{D_f} Friction drag coefficient
- J_L Jetevator lateral load coefficient
- J_D Jetevator axial load coefficient
- J_{M_f} Jetevator aerodynamic hinge moment
- M Mach number
- p Pressure
- q Dynamic pressure
- R Jetevator radius
- (x, y, z) Cartesian coordinates
- (R, φ, θ) Spherical coordinates of jetevator with radius R
- δ Jetevator deflection angle
- ψ Nozzle expansion half angle

~~CONFIDENTIAL~~ DECLASSIFIED

ANALYSIS

The analysis is divided into two parts. In the first part, expressions for lateral control effectiveness, thrust decrement, and aerodynamic hinge moments are presented for the condition wherein flow separation in the nozzle ahead of the deflected jetevator does not occur. The second section presents a similar analysis for the separated flow case.

THE UNSEPARATED FLOW CASE

Flow in the nozzle for this case is considered to be symmetrical about the centerline for all jetevator deflections. Therefore, it is necessary to consider only the load on the jetevator.

Coordinate System A system of rectangular and spherical coordinates as shown in Fig. 2 is assumed. An element of area of the jetevator is

$$dS = R^2 \sin \Phi d\Phi d\Theta \quad (1)$$

where R is the jetevator radius. The component of the elemental force on this area perpendicular to the xz plane is

$$dL = \Delta p R^2 \sin^2 \Phi \sin \Theta d\Phi d\Theta \quad (2)$$

where Δp is the pressure acting on the elemental area dS .

Pressure It is presently not possible to write an exact expression that will give the pressure distribution on the jetevator. Because of the concavity of the inner face, it is considered that the pressure can be represented by a linearized function of the flow deflection angle.

~~CONFIDENTIAL~~ DECLASSIFIED

~~CONFIDENTIAL~~ DECLASSIFIED

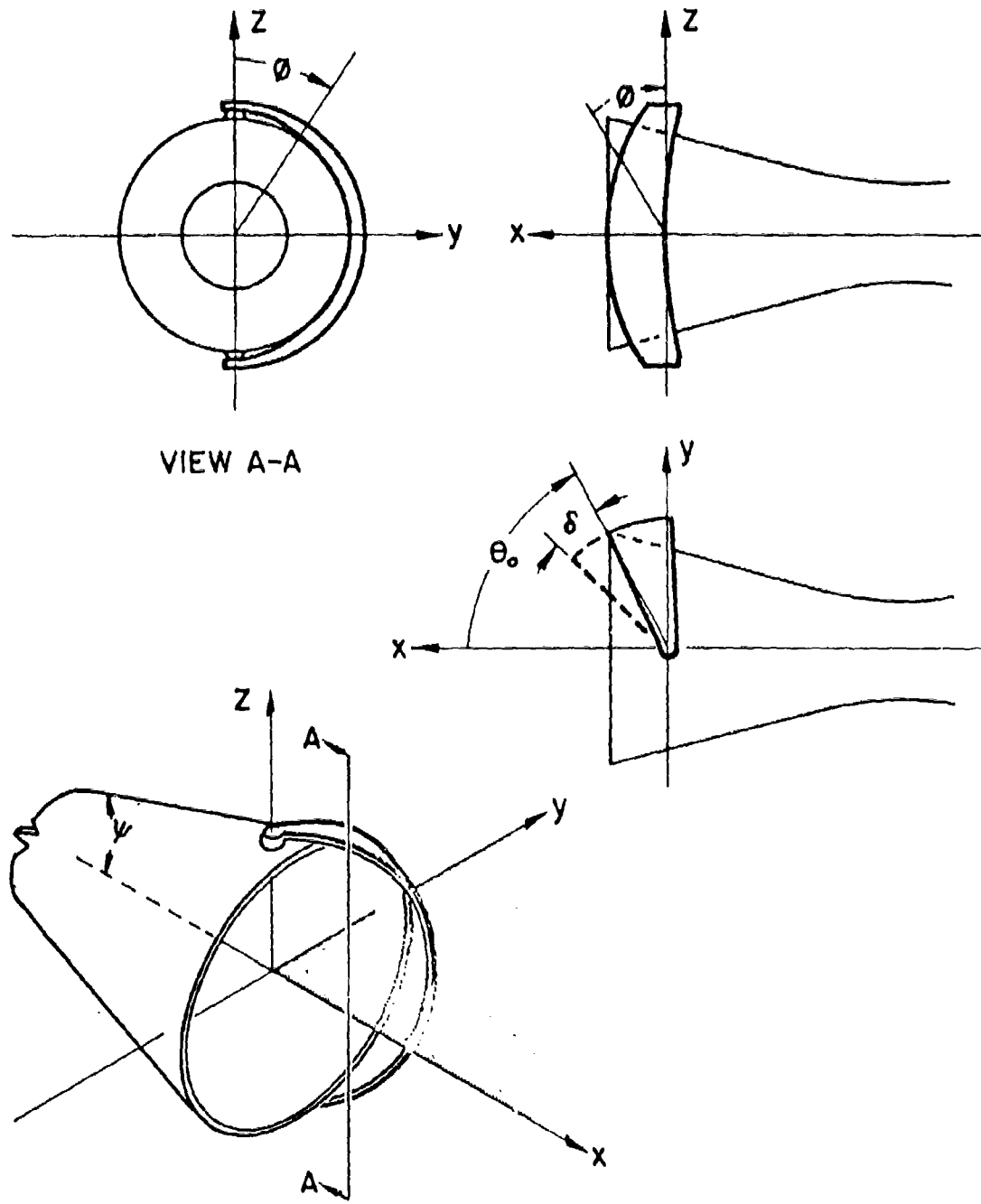


Fig. 2 Orientation of Jetevator in Cartesian Coordinate System and Spherical Coordinate System

~~CONFIDENTIAL~~ DECLASSIFIED

~~CONFIDENTIAL~~ DECLASSIFIED

Let

$$\Delta p = p_1 \left(\frac{A p}{p_1} \right) = p_1 \left(\frac{p}{p_1} - \frac{p_a}{p_1} \right) \quad (3)$$

where: p_1 - static pressure at the nozzle face for zero jetevator deflection.

p - pressure on the side of the deflected jetevator that is exposed to the nozzle exhaust gas.

p_a - pressure on the back side of the jetevator.

By expanding in a power series, the pressure in terms of the flow deflection angle is

$$\frac{p}{p_1} = \left. \frac{p}{p_1} \right|_{\theta = \theta_0} + \left. \frac{\partial \left(\frac{p}{p_1} \right)}{\partial \theta} \right|_{\theta = \theta_0} (\theta_0 - \theta) + \dots$$

The difference in pressure between the inside and back side at any point, then, is (for linear terms only)

$$\Delta p = p_1 \left[A + B(\theta_0 - \theta) - \frac{p_a}{p_1} \right] \quad (4)$$

where

$$A = \left. \frac{p}{p_1} \right|_{\theta = \theta_0}$$

$$B = \left. \frac{\partial \left(\frac{p}{p_1} \right)}{\partial \theta} \right|_{\theta = \theta_0}$$

An estimate of the value of the constants A and B can be made by considering a two-dimensional flow in the xy plane (see Fig. 2). The constant A, therefore, is the ratio of the static pressure behind the shock wave that originates at the intersection of the nozzle trailing edge and the jetevator to the static pressure just ahead of this shock wave. By applying two-dimensional shock wave theory, the increase in pressure on the inside face of the jetevator due to curvature can be

~~CONFIDENTIAL~~ DECLASSIFIED

~~CONFIDENTIAL~~ DECLASSIFIED

computed. A straight line approximation to the slope of this pressure increase with Θ is consistent with the linearization and determines the value of the constant B . As stated previously the foregoing procedure is approximately correct only for the $x\eta$ plane. Because of the concavity, however, it is believed that the approximation is reasonable for points away from this plane.

Lateral Force Substituting Eq. 4 into Eq. 2, the total force normal to the xz plane is

$$L = 2R^2 \int_{\sin^{-1} \frac{\cos \Theta_0}{\cos(\Theta_0 - \delta)}}^{\frac{\pi}{2}} \int_{\Theta_0 - \delta}^{\cos^{-1} \frac{\cos \Theta_0}{\sin \phi}} \left[A + B(\Theta_0 - \Theta) - \frac{P_0}{P_1} \right] \sin^2 \phi \sin \Theta \, d\Theta \, d\phi$$

This equation can be integrated to obtain a lateral force coefficient of effectiveness as

$$J_L = \frac{L}{P_1 R^2} = \left\{ N \left[\frac{\pi}{2} - \zeta + m \cos \zeta \right] - 2 M a \cos \zeta - B \left[\sqrt{(1-m^2)(m^2-a^2)} \right. \right. \\ \left. \left. + C - \frac{a^2+1}{2} \sin^{-1} \left(\frac{2m^2-(a^2+1)}{1-a^2} \right) - 2a(\Theta_0 - \delta) \cos \zeta \right. \right. \\ \left. \left. + a \sin^{-1} \left(\frac{(1+a^2)m^2 - 2a^2}{(1-a^2)m^2} \right) \right] \right\} \quad (5)$$

where

$$N = M \cos(\Theta_0 - \delta) + B \sin(\Theta_0 - \delta) - B(\Theta_0 - \delta) \cos(\Theta_0 - \delta)$$

$$M = A + B\Theta_0 - \frac{P_0}{P_1}$$

~~CONFIDENTIAL~~ DECLASSIFIED

~~CONFIDENTIAL~~ DECLASSIFIED

$$m = \frac{\cos \Theta_0}{\cos(\Theta_0 - \delta)}$$

$$\gamma = \sin^{-1} m = \sin^{-1} \frac{a}{\cos(\Theta_0 - \delta)}$$

$$a = \cos \Theta_0$$

$$C = \frac{\pi}{4} [(a^2 + 1) - 2a]$$

Upon examining Eq. 5, it can be seen that the lateral force coefficient, J_L , is a function of A , B , $\frac{P_a}{P_1}$, δ and Θ_0 . The dependence upon δ , of course, needs no discussion. The parameter Θ_0 essentially defines the position of the jetvator hinge relative to the nozzle face. The two pressure parameters, A and B , are functions of the Mach number at the nozzle face and the ratio of specific heats for the rocket gas; they are related to the nozzle design as well as the jetvator design. The ratio $\frac{P_a}{P_1}$ is retained as a parameter to account for the fact that the pressure on the back side of the jetvator is a function of ambient pressure as well as the missile base pressure which is influenced by the speed.

Thrust Decrement With reference to Fig. 2 again, the component of the elemental force on the area dS (see Eq. 1) perpendicular to the yz plane is

$$dD = \Delta p R^2 \sin^2 \phi \cos \Theta d\Theta d\phi \tag{6}$$

Upon substitution for Δp from Eq. 4, the total force in the x direction is

$$D = 2 P_1 R^2 \int_{\sin^{-1} \frac{\cos \Theta_0}{\cos(\Theta_0 - \delta)}}^{\frac{\pi}{2}} \int_{(\Theta_0 - \delta)}^{\cos^{-1} \frac{\cos \Theta}{\sin \phi}} \left[A + B(\Theta_0 - \Theta) - \frac{P_a}{P_1} \right] R^2 \sin^2 \phi \cos \Theta d\Theta d\phi$$

~~CONFIDENTIAL~~ DECLASSIFIED

~~CONFIDENTIAL~~ DECLASSIFIED

or

$$D = 2\rho_1 R^2 \int_0^{\frac{\pi}{2}} \frac{1}{\sin^{-1} \frac{\cos \theta_0}{\cos(\theta_0 - \delta)}} \left\{ M \sqrt{\sin^2 \varphi - \cos^2 \theta_0} \sin \varphi + N_0 \sin^2 \varphi \right. \\ \left. - B \cos \theta_0 \sin \varphi - B \sqrt{\sin^2 \varphi - \cos^2 \theta_0} \left[\cos^{-1} \left(\frac{\cos \theta_0}{\sin \varphi} \right) \sin \varphi \right] \right\} d\varphi \quad (7)$$

The last term in Eq. 7 was expanded in powers of $\sin \varphi$ and integrated term by term. Terms up to and including the seventh power were retained. From Eq. 7, then, a coefficient of thrust decrement can be defined as

$$J_D = \frac{D}{\rho_1 R^2} = M \left[\sqrt{(1-m^2)(m^2-a^2)} + \frac{(1-a^2)}{2} \cos^{-1} \left(\frac{2m^2 - (1+a^2)}{1-a^2} \right) \right] \\ + N_0 \left[\cos^{-1} m + m \sqrt{1-m^2} \right] - 2B \left[K_1 \cos^{-1} m + K_3 m \sqrt{1-m^2} \right. \\ \left. - K_4 \log_e \left(\frac{1-\sqrt{1-m^2}}{m} \right) - K_5 \frac{\sqrt{1-m^2}}{m} + K_6 \frac{\sqrt{1-m^2}}{m^2} \right. \\ \left. - K_7 \frac{\sqrt{1-m^2}}{m^3} + K_8 \frac{\sqrt{1-m^2}}{m^4} \right] \quad (8)$$

where

$$M = A + B \theta_0 - \frac{P_A}{P_1}$$

$$N_0 = B \cos(\theta_0 - \delta) - M \sin(\theta_0 - \delta) + B(\theta_0 - \delta) \sin(\theta_0 - \delta)$$

$$a = \cos \theta_0$$

~~CONFIDENTIAL~~ DECLASSIFIED

$$m = \frac{\cos \theta_0}{\cos (\theta_0 - \delta)}$$

$$K_1 = \frac{\pi}{4} (1 - a^2)$$

$$K_3 = \frac{\pi}{4}$$

$$K_4 = \frac{a^3}{5} + \frac{a^5}{15} + \frac{a^7}{35}$$

$$K_5 = \frac{\pi}{16} (a^4 + \frac{a^6}{9})$$

$$K_6 = \frac{a^5}{15} + \frac{a^7}{35}$$

$$K_7 = \frac{\pi}{96} a^6$$

$$K_{\theta} = \frac{2}{105} a^7$$

From a comparison of Eqs. 5 and 8, it can be determined that J_D and J_L are functions of the same parameters.

Aerodynamic Hinge Moment Since the jetevator is spherical, pressures upon the surface exposed to the rocket exhaust result in a load that passes through the hinge line and, theoretically, contribute no hinge moment. Moments about the hinge will be caused, however, by the frictional drag of the exhaust gases upon the inside face of the jetevator and also by pressures acting along the trailing edge surface. In this section only the frictional hinge moment is considered.

The moment of the frictional force on the element of area dS (Eq. 1) is

$$dM_f = C_{Df} q R^3 \sin^2 \varphi d\theta d\varphi \quad (9)$$

~~CONFIDENTIAL~~ DECLASSIFIED

where

q is the dynamic pressure at the nozzle face and
 C_{D_f} is the friction drag coefficient based upon q and the
 area of the jetevator face exposed to the exhaust stream.

The total frictional hinge moment is

$$M_f = 2 C_{D_f} q R^3 \int_{\sin^{-1} \frac{\cos \Theta_0}{\cos(\Theta_0 - \delta)}}^{\frac{\pi}{2}} \int_{(\Theta_0 - \delta)}^{\cos^{-1} \frac{\cos \Theta}{\sin \phi}} \sin^2 \phi \, d\Theta \, d\phi \quad (10)$$

or

$$M_f = 2 C_{D_f} q R^3 \left\{ \int_{\sin^{-1} \frac{\cos \Theta_0}{\cos(\Theta_0 - \delta)}}^{\frac{\pi}{2}} \left[\cos^{-1} \left(\frac{\cos \Theta}{\sin \phi} \right) \right] \sin^2 \phi \, d\phi - (\Theta_0 - \delta) \int_{\sin^{-1} \frac{\cos \Theta_0}{\cos(\Theta_0 - \delta)}}^{\frac{\pi}{2}} \sin^2 \phi \, d\phi \right\} \quad (10)$$

The first term in Eq. 10 was expanded in powers of $\sin \phi$ and terms up to and including the seventh power were retained. After integrating term by term the following expression is obtained.

$$J_{M_f} = \frac{M_f}{q R^3} = C_{D_f} \left\{ \left[\frac{\pi}{2} - (\Theta_0 - \delta) \right] \left[\frac{\pi}{2} - \bar{\gamma} + m \cos \bar{\gamma} \right] - 2 a \cos \bar{\gamma} \right. \\ \left. - \frac{\cos \bar{\gamma}}{m^2} k_1 - k_2 \frac{\cos \bar{\gamma}}{m} + k_3 \log_e \left(\frac{1 - \cos \bar{\gamma}}{m} \right) \right\} \quad (11)$$

where

$$\bar{\gamma} = \sin^{-1} \frac{\cos \Theta_0}{\cos(\Theta_0 - \delta)}$$

$$m = \frac{\cos \Theta_0}{\cos(\Theta_0 - \delta)}$$

~~CONFIDENTIAL~~ DECLASSIFIED

~~CONFIDENTIAL~~ DECLASSIFIED

$$a = \cos \theta_0$$

$$K_1 = \frac{a^5}{2240} (168 + 75 a^2)$$

$$K_2 = \frac{15 a^4}{672}$$

$$K_3 = a^3 \left[\frac{1}{3} + \frac{3a^2}{40} + \frac{15a^4}{448} \right]$$

THE SEPARATED FLOW CASE

Near the wall of the rocket nozzle, a gradient in velocity exists, and the resulting shears in this region cause a boundary layer of some undetermined thickness. Since a favorable pressure gradient exists in the nozzle, this layer would be expected to be quite thin. However, it is true that in the subsonic portions of the boundary layer pressure pulses from downstream can move up into the nozzle. Thus it is that the increase in pressure associated with the deflected jetevator can be felt upstream and a boundary layer separation point can be established at some point in the nozzle ahead of the deflected jetevator. The assumptions associated with the prediction of the pressures existing on the jetevator and upon the nozzle in the presence of a separated boundary layer are discussed in the following section.

Pressure Most experimental and analytical studies of shock-induced boundary layer separation pertain to air and generally do not consider a favorable pressure gradient such as exists in a rocket nozzle (see Refs. 3 and 4). Nevertheless, the assumption is made herein that existing data regarding shock-induced separation for air can be applied to rocket gases. More specifically, the increase in pressure associated with flow separation at various Mach numbers can be estimated by examining published data for air. Accordingly, pertinent

~~CONFIDENTIAL~~ DECLASSIFIED

~~CONFIDENTIAL~~ DECLASSIFIED

parameters as determined from wind tunnel tests are plotted in Fig. 3. The data given in this figure indicate that the pressure jump across the shock wave induced by the boundary layer separation is a function primarily of Mach number. The equivalent wedge formed by the separated flow varies approximately between 14° and 16° .

Schematic sketches of the flow with boundary layer separation is shown in Figs. 4 and 5. The most forward point within the nozzle at which the boundary layer is separated is Point 2 in Fig. 5. The point (in the xy plane) at which the surface of discontinuity (assumed to be conical) between the separated flow and unseparated flow intersects the jetevator is Point 4 in Fig. 5. For computational purposes it is assumed that the pressure along the surface of discontinuity can be taken as an average pressure, P_{SAV} , between that behind the shock at Point 2 and the pressure p which would exist at the face of the nozzle (for no jetevators). This pressure, therefore, acts on the nozzle as well as on part of the jetevator. For the pressure along the jetevator behind Point 4, the Mach number M , and static pressure p , was considered to define the flow ahead of the shock at Point 4, and the effects of the turning of the flow from Point 4 to the jetevator trailing edge was computed two-dimensionally as in the unseparated case.

The separation pattern within the nozzle is difficult to determine uniquely. For purposes of mathematical analysis, it was assumed that in the side view the separation boundary in the nozzle is a straight line drawn from the most forward point (Point 2 in Fig. 5) to the point at which the jetevator aft edge intersects the nozzle lip (Point 1 in Fig. 5). As previously mentioned, the surface of discontinuity defining the separated layer was assumed to be conical and was considered to subtend equal wedge angles measured from the nozzle wall in any plane passing through the nozzle centerline. With these boundary conditions, then, a procedure for estimating the lateral and axial forces upon the nozzle and jetevator is given in the following paragraphs.

Lateral Force on the Nozzle With reference to Fig. 5, consider that a plane parallel to the z -axis passes through Points 1 and 2. The parametric equations for the intersection of this plane and the conical nozzle are

13
~~CONFIDENTIAL~~ DECLASSIFIED

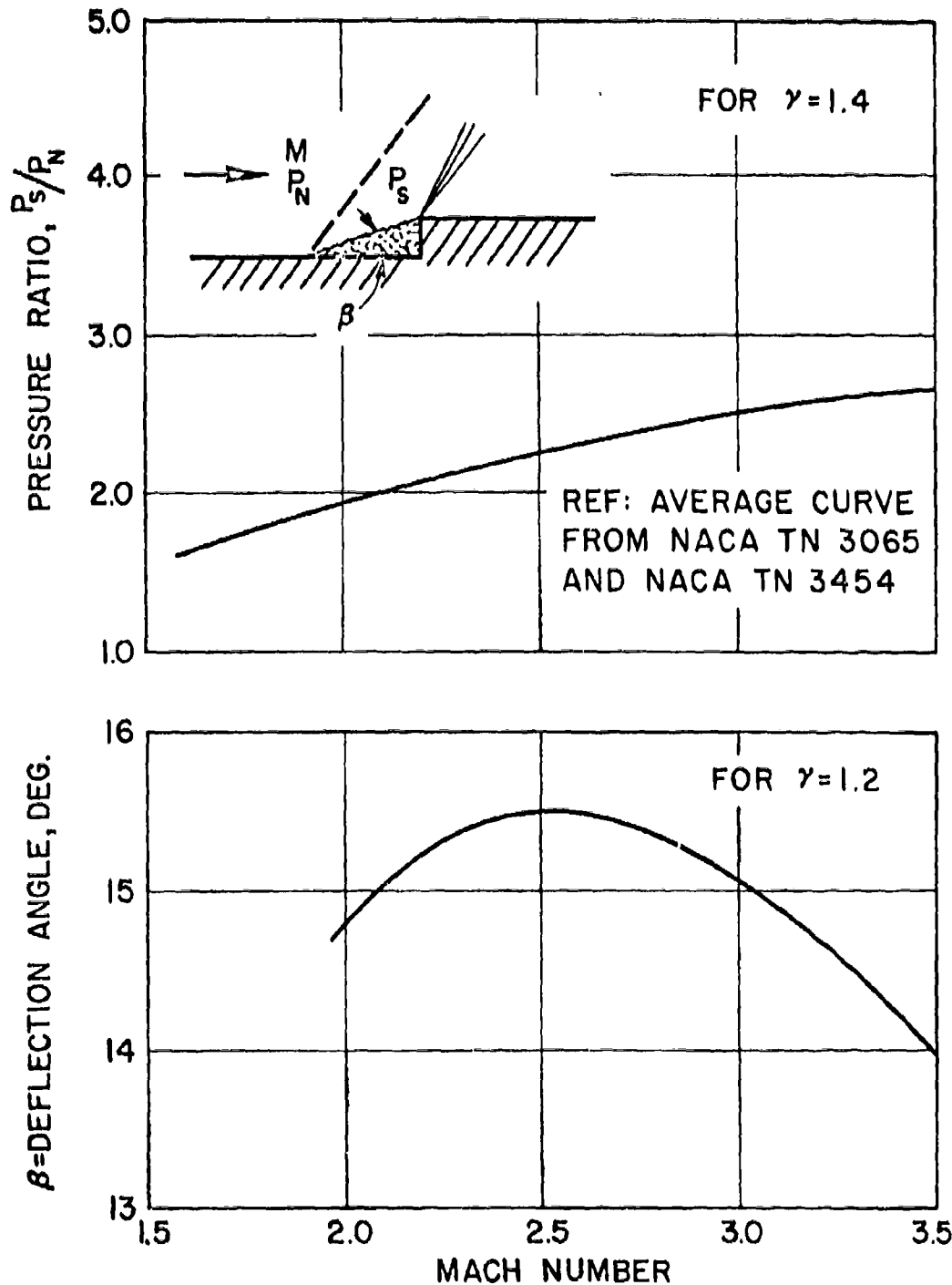


Fig. 3 Criteria for Establishing Strength of Shock Due to Flow Separation

~~CONFIDENTIAL~~ CLASSIFIED

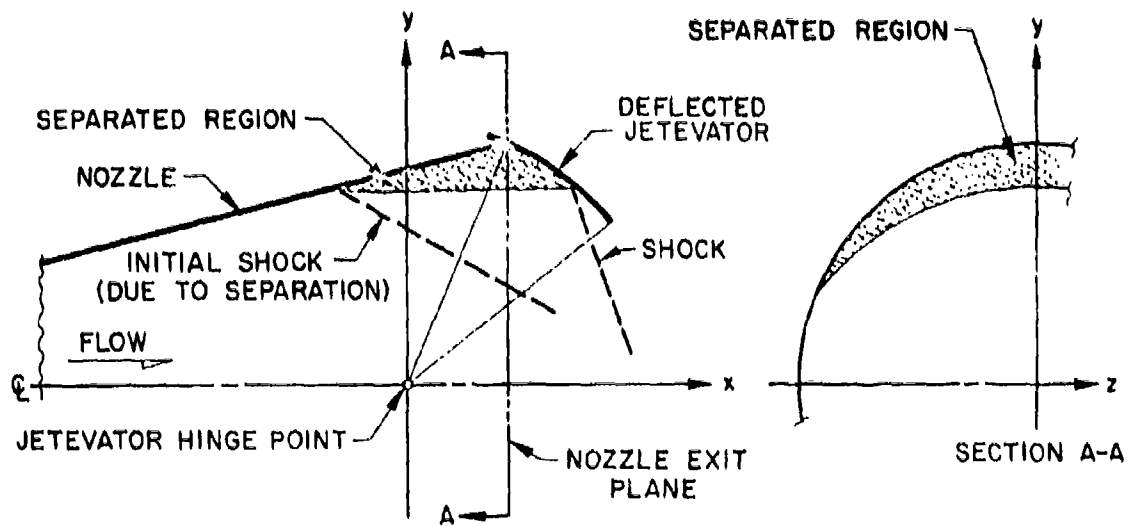


Fig. 4 Model for the Analysis of Separated Flow Case

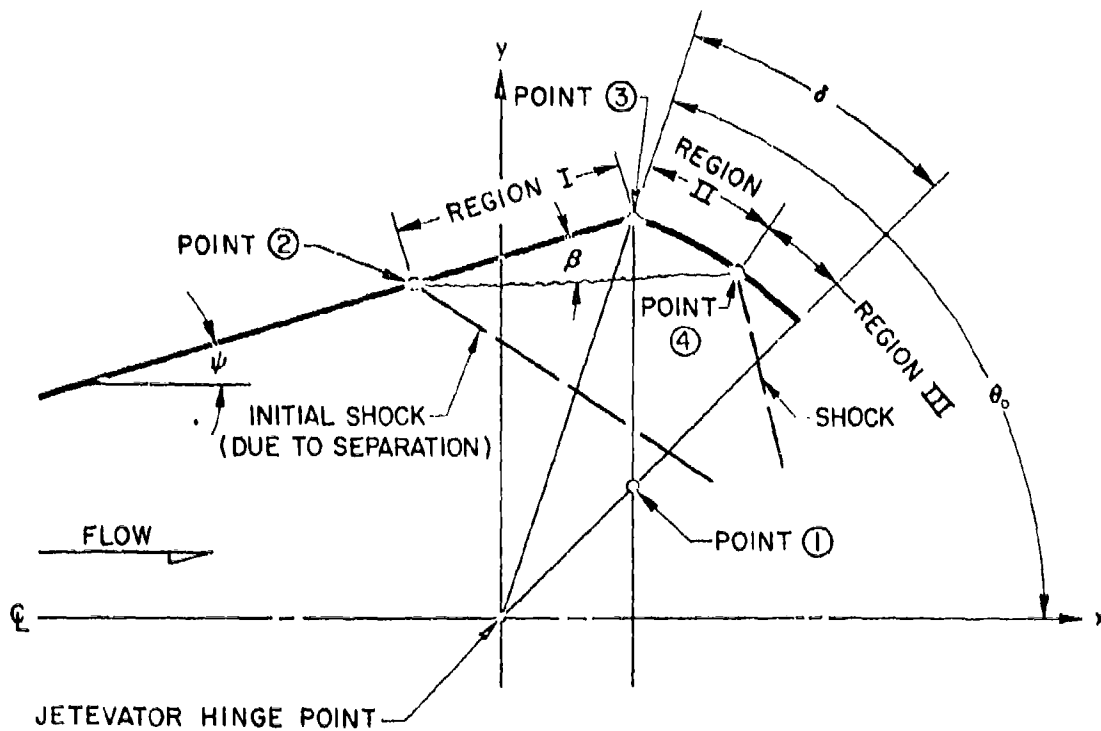


Fig. 5 Schematic of Separated Flow Case with Definitions

~~CONFIDENTIAL~~ CLASSIFIED

~~CONFIDENTIAL~~
~~CLASSIFIED~~

$$[(x - x_0) \tan \psi]^2 = y^2 + z^2 \quad (12)$$

$$y = \bar{m}x + h \quad (13)$$

If we consider, then, only values of y defined by Eq. 13, and equation for the corresponding z as a function of x can be obtained as

$$[(x - x_0) \tan \psi]^2 = (\bar{m}x + h)^2 + z^2 \quad (14)$$

The line defined by Eq. 14 is in the xz plane and represents the projection of the boundary-layer separation points in the nozzle upon the xz plane. Equation 14 is an ellipse.

It is assumed that a constant pressure $P_{S_{AV}}$ acts outward on the conical nozzle within the boundaries of the separated flow region. In order to find the lifting pressure contributing to the load on the nozzle, the pressure $P_{S_{AV}}$ must be compared to the pressure that normally would exist in the separated portion of the nozzle had separation not occurred. Accordingly, the increment in pressure contributing to the load is

$$\Delta p = p_i \left(\frac{P_{S_{AV}}}{P_i} - \frac{P_{n_{AV}}}{P_i} \right) \quad (15)$$

where

p_i = static pressure at the nozzle exit area for unseparated flow.

$P_{S_{AV}}$ = average pressure in the separated flow region as influenced by the increase in pressure caused by the shock wave associated with the boundary layer separation.

$P_{n_{AV}}$ = the normal unseparated flow pressures in the nozzle averaged for the area of the nozzle covered by separated flow.

~~CONFIDENTIAL~~
DECLASSIFIED

These outward pressures are inclined forward by the angle ψ (nozzle expansion half-angle) relative to the x axis.

To compute the lateral load on the nozzle, the pressure multiplied by the cosine of the angle ψ is integrated over the separated area of the nozzle projected to the xz plane. This area (Region I in Fig. 5) is bounded by the line given in Eq. 14 and the line parallel to the z axis defined by $y=0$ and $x = R \cos \Theta_0$.

The load, then, is

$$L_1 = 2 \Delta p \cos \psi \int_{x_2}^{x_1} \int_0^{\sqrt{(x-x_0)^2 \tan^2 \psi - (\bar{m}x+h)^2}} dz dx$$

This equation can be integrated to obtain

$$L_1 = \frac{\Delta p \cos \psi}{c} \left\{ \left[[cx_1 - (x_0 \tan^2 \psi + \bar{m}h)] \sqrt{cx_1^2 + bx_1 + a} \right. \right. \\ \left. \left. - [cx_2 - (x_0 \tan^2 \psi + \bar{m}h)] \sqrt{cx_2^2 + bx_2 + a} \right] \right. \\ \left. + \frac{(\tan^2 \psi)}{\sqrt{c}} (h + \bar{m}x_0)^2 \left\{ \sin^{-1} \left[\frac{cx_1 - (x_0 \tan^2 \psi + \bar{m}h)}{(\tan \psi)(h + \bar{m}x_0)} \right] - \sin^{-1} \left[\frac{cx_2 - (x_0 \tan^2 \psi + \bar{m}h)}{(\tan \psi)(h + \bar{m}x_0)} \right] \right\} \right\} \quad (16)$$

~~CONFIDENTIAL~~
DECLASSIFIED

~~CONFIDENTIAL~~ ~~CLASSIFIED~~

where

x_0 is the x-distance of the nozzle cone vertex from the origin of the x, y, z coordinate system (jetevator hinge).

x_2 is the x-coordinate of the foremost point of boundary layer separation in the nozzle ahead of the jetevator.

x_1 is the x-coordinate of the intersection of the jetevator trailing edge and the nozzle lip.

$$a = (x_0^2 \tan^2 \psi - h^2)$$

$$b = -2(x_0 \tan^2 \psi + \bar{m}h)$$

$$c = (\tan^2 \psi - \bar{m}^2)$$

$$\bar{m} = -\tan \eta = \frac{y_2 - y_1}{x_2 - x_1}$$

y_2 is the y-coordinate of the boundary layer separation point.

y_1 is the y-coordinate of the jetevator trailing edge and the nozzle lip.

$$h = y_1 + R \cos \theta_0 \tan \eta$$

For computing purposes, it is convenient to express Eq. 16 non-dimensionally. Accordingly, therefore, if all lengths are divided by R (the jetevator radius), a coefficient of lateral effectiveness can be defined as

~~CONFIDENTIAL~~

$$J_L = \frac{L}{PR^2} = \left[\frac{P_{SAV}}{P_1} - \frac{P_{NAV}}{P_1} \right] \frac{\cos \psi}{c} \left\{ G_1 \sqrt{E_1} - G_2 \sqrt{E_2} \right. \\ \left. + \frac{F^2 \tan^2 \psi}{\sqrt{-c}} \left[\sin^{-1} \left(\frac{G_1}{F \tan \psi} \right) - \sin^{-1} \left(\frac{G_2}{F \tan \psi} \right) \right] \right\} \quad (17)$$

where

$$a = (x_0')^2 \tan^2 \psi - h^2$$

$$b = -2(x_0' \tan^2 \psi + \bar{m}h)$$

$$c = \tan^2 \psi - \bar{m}^2$$

$$D = x_0' \tan^2 \psi + \bar{m}h$$

$$E_1 = c(x_1')^2 + b(x_1') + a$$

$$E_2 = c(x_2')^2 + b(x_2') + a$$

$$F = h + \bar{m}x_0'$$

$$G_1 = cx_1' - D$$

$$G_2 = cx_2' - D$$

$$h = y_1' - \bar{m} \cos \Theta_0$$

$$\bar{m} = \frac{y_2 - y_1}{x_2 - x_1}$$

$$x_0' = \frac{x_0}{R} = -\frac{\sin \Theta_0}{\tan \psi} = \cos \Theta_0$$

$$x_1' = \frac{x_1}{R} = \cos \Theta_0$$

$$x_2' = \frac{x_2}{R} \text{ (given)}$$

$$y_1' = \frac{y_1}{R} = \cos \theta_0 \tan (\theta_0 - \delta)$$

$$y_2' = \frac{y_2}{R} = x_2' \tan \psi + \sin \theta_0 (1 - \cot \theta_0 \tan \psi)$$

Lateral Force on the Jetevator To estimate the loads on the jetevator, it is assumed first that the general level of the static pressure in Region II of Fig. 5 is P_{3AV} . As a first contribution to the lateral force on the jetevator, it was considered that a constant pressure equal to P_{3AV} acted upon the total inner surface. Upon examining Eq. 5, the contribution of this pressure to the lateral load coefficient is

$$J_{L_2} = \frac{L_{L_2}}{P_1 R^2} = N_2 \left(\frac{\pi}{2} - \bar{x} + m_2 \cos \bar{x} \right) - 2 M_2 a_2 \cos \bar{x} \quad (18)$$

where B in Eq. 5 is zero

$$N_2 = M_2 \cos (\theta_0 - \delta)$$

$$M_2 = \left(A_2 - \frac{P_a}{P_1} \right) \left(\frac{P_{3AV}}{P_1} - \frac{P_a}{P_1} \right)$$

In Region III (Fig. 5) an increase in pressure above that in Region II occurs first due to the shock wave at Point 4 and then to the effect of the jetevator curvature in Region III. To compute the contribution of the pressures in this region to the jetevator lateral load, Eq. 5 was altered so that it would apply only for Region III. To accomplish this, the angle θ_0 in Eq. 5 is redefined as the angle measured from the y axis to a line drawn from the hinge point to Point 4 in Fig. 5. Correspondingly, the angle δ is measured from this new θ_0 . The pressure in Region III was determined by assuming that the static pressure and Mach number ahead of the shock at Point 4 was equal to the value that would exist at the nozzle face for zero

~~CONFIDENTIAL~~ ~~CLASSIFIED~~

jetevator deflection. Again, two-dimensional flow considerations were used to estimate the terms A and B in Eq. 4. By appropriately altering the parameters in Eq. 5 then the contribution of Region III is

$$\begin{aligned}
 J_{L_3} = \frac{L_3}{R^2} = & N_3 \left(\frac{\pi}{2} - \bar{\alpha}_3 + m_3 \cos \bar{\alpha}_3 \right) - 2 M_3 a_3 \cos \bar{\alpha}_3 - B_3 \left[\sqrt{(1-m_3)^2 (m_3^2 - a_3^2)} \right. \\
 & + C_3 - \left(\frac{a_3^2 + 1}{2} \right) \sin^{-1} \left(\frac{2m_3^2 - (a_3^2 + 1)}{1 - a_3^2} \right) - 2 a_3 (\cos \bar{\alpha}_3) (\Theta_{o_3} - \delta_3) \quad (19) \\
 & \left. + a_3 \sin^{-1} \left(\frac{(1 + a_3^2) m_3^2 - 2 a_3^2}{(1 - a_3^2) m_3^2} \right) \right]
 \end{aligned}$$

Total Lateral Load The total lateral load coefficient contributed by the three regions is

$$J_L = J_{L_1} + J_{L_2} + J_{L_3} \quad (20)$$

Axial Force on the Nozzle The pressure Δp given in Eq. 15 exerts an axial force on the nozzle in the forward direction and tends to reduce the overall thrust decrement. To compute this force let ds_1 be an element of cone area and ds be the projection of this area on the xz plane.

Then

$$ds_1 = ds \sec \beta$$

where β is the direction cosine associated with the outward normal to ds , in the y direction. From the equation for the conical nozzle

$$\sec \beta = \frac{\sqrt{x^2 + y^2 + [(x - x_0)^2 \tan^2 \psi]^2}}{y}$$

~~CONFIDENTIAL~~ ~~CLASSIFIED~~

The radial force on the conical portion of the nozzle is $\iint_{S_1} \Delta p ds_1$
 The axial component of this force is

$$D = \sin \psi \iint_{S_1} \Delta p ds_1 = \Delta p \sin \psi \iint_{S_1} \frac{\sqrt{z^2 + y^2 + [(x-x_0)\tan\psi]^2}}{y} dy dz$$

For the boundary conditions of the separated flow region previously discussed

$$y = \sqrt{[(x-x_0)\tan\psi]^2 - z^2}$$

and

$$D = \Delta p \sin \psi \tan \psi \iint_{S_1} \frac{\sqrt{(x-x_0)^2 + (x+x_0)^2 \tan^2 \psi}}{(x-x_0)^2 \tan^2 \psi - z^2} dx dz$$

Let $t = x - x_0$ then

$$D = 2 \Delta p \sin \psi \tan \psi \int_{x_2-x_0}^{x_1-x_0} \frac{1}{\sqrt{1+\tan^2 \psi}} + \left\{ \int_0^{\sqrt{a_1^2 t^2 - [\bar{m}(t+x_0)+h]^2}} \frac{dz}{\sqrt{t^2 \tan^2 \psi - z^2}} \right\} dt \quad (21)$$

Equation 21 was integrated to obtain an axial force coefficient equal to

$$\begin{aligned} J_{D_1} = -\frac{D_1}{P_1 R^2} = & - \left(\frac{P_{S_{AV}}}{P_1} - \frac{P_{N_{AV}}}{P_1} - \frac{P_{A_0}}{P_1} \right) \tan^2 \psi \left\{ \left[(x_1-x_0)^2 \right. \right. \\ & \left. \left. \sin^{-1} \left(\frac{\sqrt{a_1 + b_1(x_1-x_0) + c_1(x_1-x_0)^2}}{(x_1-x_0)\tan\psi} \right) \right] - \left[(x_2-x_0)^2 \sin^{-1} \frac{\sqrt{a_1 + b_1(x_2-x_0) + c_1(x_2-x_0)^2}}{(x_2-x_0)\tan\psi} \right] \right\} \\ & - \frac{\bar{m}}{c_1} \left\{ \sqrt{a_1 + b_1(x_1-x_0) + c_1(x_1-x_0)^2} - \sqrt{a_1 + b_1(x_2-x_0) + c_1(x_2-x_0)^2} \right\} \quad (22) \\ & + \frac{\bar{m}^2}{c_1 \sqrt{c_1}} \left\{ \sin^{-1} \left[\frac{-\bar{m}n + c_1(x_1-x_0)}{n \tan \psi} \right] - \sin^{-1} \left[\frac{-\bar{m}n + c_1(x_2-x_0)}{n \tan \psi} \right] \right\} \end{aligned}$$

where all linear coordinates are in terms of the jetevator radius as in Eq. 15 and where

$$\begin{aligned} a_1 &= -n^2 = -(\bar{m}x_0 + h)^2 \\ b_1 &= -2\bar{m}n = -2(\bar{m}^2x_0 + \bar{m}h) \\ c_1 &= \tan^2\psi - \bar{m}^2 \\ n &= \bar{m}x_0 + h \end{aligned}$$

Axial Force on the Jetevator To estimate the axial force on the jetevator, the parameters in Eq. 8 were modified in a manner analogous to the modifications to Eq. 5 that were made to obtain the lateral force. More specifically

$$\begin{aligned} J_{D_2} = \frac{D_{2z}}{\rho_1 R^2} = M_2 \left[\sqrt{(1-m_2^2)(m_2^2-a_2^2)} + \left(\frac{1-a_2^2}{2}\right) \cos^{-1} \left(\frac{2m_2^2-1-a_2^2}{1-a_2^2}\right) \right. \\ \left. + N_{D_2} (\cos^{-1} m_2 + m_2 \sqrt{1-m_2^2}) \right] \end{aligned} \quad (23)$$

where B in Eq. 8 is zero

$$\begin{aligned} N_{D_2} &= -M_2 \sin(\theta_0 - \delta) \\ M_2 &= \left(A - \frac{p_a}{\rho_1}\right) - \left(\frac{p_{x_{av}}}{\rho_1} - \frac{p_a}{\rho_1}\right) \end{aligned}$$

~~CONFIDENTIAL~~ DECLASSIFIED

and

$$\begin{aligned}
 J_{03} - \frac{D_A}{P_t R^2} = & M_3 \left[\sqrt{(1-m_3^2)(m_3^2-a_3^2)} + \frac{(1+a_3^2)}{2} \cos^{-1} \left(\frac{2m_3^2 - (1+a_3^2)}{1-a_3^2} \right) \right] \\
 & + N_{03} \left[\cos^{-1} m_3 + m_3 \sqrt{1-m_3^2} \right] - 2B_3 \left[K_1 \cos^{-1} m_3 \right. \\
 & - K_3 m_3 \sqrt{1-m_3^2} - K_4 \text{Log}_e \left(\frac{1-\sqrt{1-m_3^2}}{m_3} \right) \quad (24) \\
 & - K_5 \frac{\sqrt{1-m_3^2}}{m_3} + K_6 \frac{\sqrt{1-m_3^2}}{m_3^2} - K_7 \frac{\sqrt{1-m_3^2}}{m_3} \\
 & \left. + K_8 \frac{\sqrt{1-m_3^2}}{m_3^2} \right]
 \end{aligned}$$

~~CONFIDENTIAL~~ ~~DECLASSIFIED~~

1MSD-1030

EXPERIMENTAL RESULTS

In developing the mathematical model for analysis purposes, it was apparent that many of the assumptions would require experimental investigation. Several of the more important points requiring clarification were:

1. Pressure distribution on the deflected jetevator.
2. Pressure distribution and nature of the separated flow region in the nozzle.
3. The influence of nozzle and jetevator geometry on the above items.

Moreover, it was desirable, of course, to check the loads predicted by the analytical results with experimental values for a jetevator under actual operating conditions. It was considered that useful tests could be conducted on a model using air as the test medium, thereby separating the material heating problems and the jetevator effectiveness computations. Accordingly, therefore, a series of "cold-flow" tests were devised for purposes of obtaining pressure distribution data. These results are discussed herein together with limited test results from actual rocket firings.

Description of the Tests The cold-flow jetevator tests were conducted in the engine test cells of the Ordnance Aerophysics Laboratory at Dagingfield, Texas. A photograph and schematic drawing of the test setup are presented in Figs. 6 and 7. The model consisted of a conical nozzle, a series of semi-jetevators of various radii, and equipment for positioning the jetevator. The nozzle was designed for Mach number 3 at the exit plane. The exit diameter of the nozzle was 9.4 in and the total divergence angle was 20° . The jetevator chord was approximately 4 in. at the center line, jetevator position, with respect to the nozzle exit, was controlled by means of a hydraulic actuator.

~~CONFIDENTIAL~~ ~~DECLASSIFIED~~



Fig. 6 "Cold Flow" Jetevator Test Setup

~~CONFIDENTIAL~~ CLASSIFIED

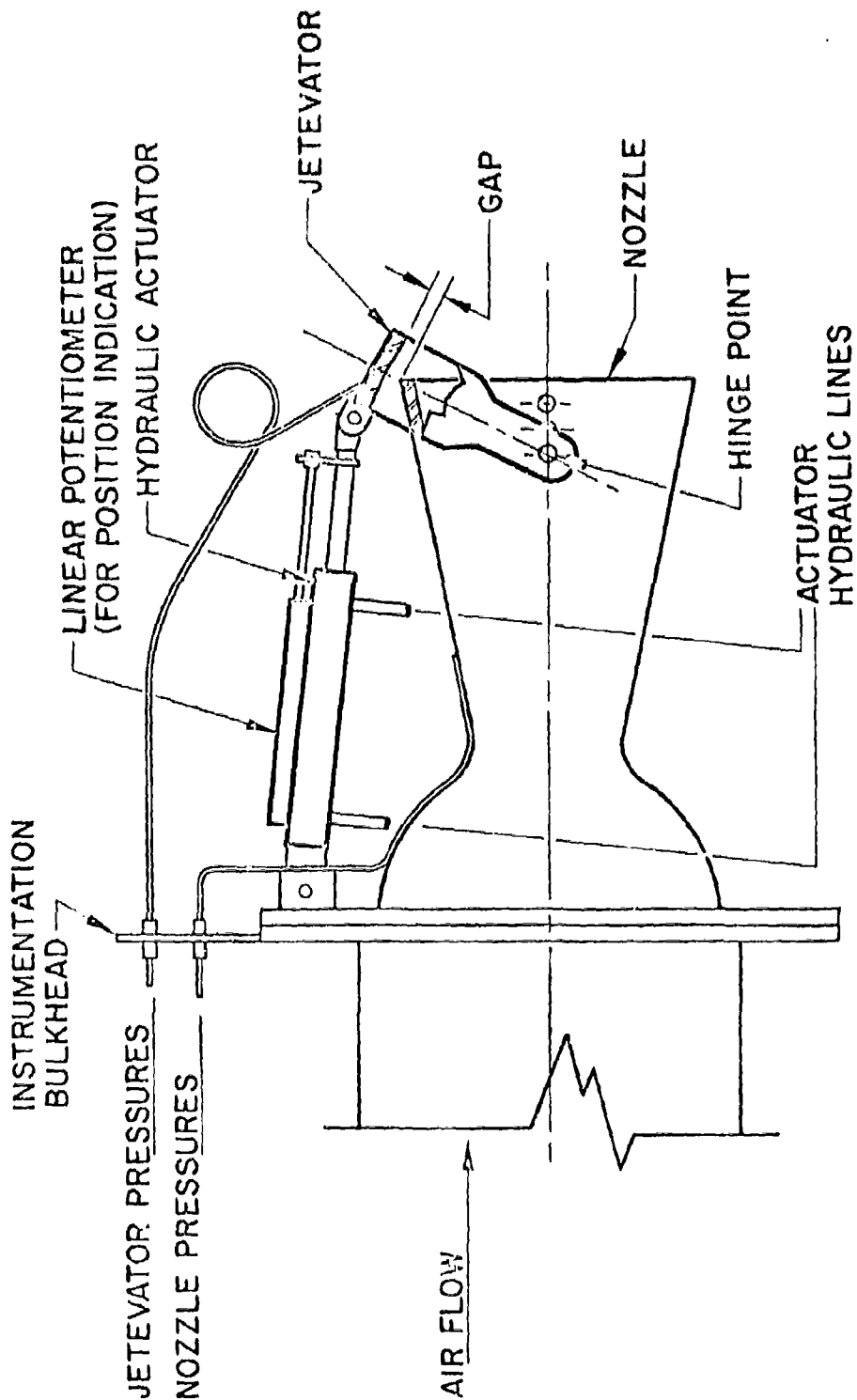


Fig. 7 Schematic of "Cold Flow" Jetevator Test Setup

~~CONFIDENTIAL~~ CLASSIFIED

~~CONFIDENTIAL~~
~~UNCLASSIFIED~~

The analytical investigation indicated that the effects of several factors could be important in jetevator design. Hinge position relative to the nozzle exit face, possible boundary layer control by means of increased gap between the nozzle lip and jetevator, and thickness of the nozzle trailing edge were considered to be of primary importance. Means of examining the influence of these parameters were, therefore, incorporated into the design. Removable fittings were provided as a means of varying the hinge point axially. Details of the fittings are shown in Fig. 6. The gap between the nozzle lip and the inner surface of the jetevator could be varied by removing special rings fitted to the nozzle and also by using jetevators of varying radii. Finally, the nozzle trailing edge thickness was varied by changing the special rings mentioned above.

Data recorded during the test consisted, primarily, of pressures from approximately 50 static orifices located in the jetevator and nozzle. The jetevator remained in a fixed position while the data were recorded to allow the use of gages and multi-manometers to measure pressure. All tests were made at a supply air temperature of 500°F. Supply pressures were 45 and 210 psia, as noted on the figures. The cell pressure was adjusted to give a ratio of supply pressure to cell pressure of approximately 37.

Test Results Results from the cold-flow tests and from representative pressure distribution data obtained by Aerojet-General Corp. during rocket motor firings confirm, in general, the fundamental assumptions utilized in the analysis. The comparison of pressure distribution data measured along the surfaces of the nozzle and jetevator on the cold-flow model with assumed pressure distributions in the analytical model is summarized as follows:

1. Without some means of boundary layer control, separation occurs in the nozzle ahead of the deflected jetevator. The deflection angle at which this separation starts is approximately 12°.

~~CONFIDENTIAL~~ UNCLASSIFIED

2. Based on values of pressure ratio across the shock, the strength of the shock wave generated by the separated flow in the nozzle is 22% higher than predicted (see Fig. 8).
3. The boundary formed by the actual flow is such that compression on the jetevator occurs along a length of the chord rather than through a strong shock as assumed in the analysis (see Fig. 8). This tends to move the area of high loading downstream on the jetevator and causes a higher axial load (thrust decrement) than predicted.
4. The pressure on the jetevator surface is maximum along the centerline but decreases toward the hinge-point. Figure 9 shows radial pressure distribution of the peak pressure points on the jetevator and nozzle as compared to assumed values. The difference in radial distribution is not considered significant, however, since the lateral load-per-unit area decreases as a function of the cosine of the radial angle.

A comparison of predicted lateral loads with loads measured during rocket motor firings also indicates that the analytical flow model is in reasonable agreement with test data. Figure 10 shows curves of lateral load as a function of jetevator deflection for unseparated and separated flow cases as computed from Eqs. 5 and 20, respectively. These computations have been made for a particular nozzle-jetevator system with the dimensions listed on the figure and corresponds to a configuration tested by the Aerojet-General Corp. during a rocket motor firing. The results of this test are also shown on the figure.

The effects of changes in geometry were determined by comparison of pressure distributions. The pressure data were also integrated over the nozzle and jetevator to give lateral and axial loads for selected configurations. One of the important parameters in the analysis was location

~~CONFIDENTIAL~~ UNCLASSIFIED

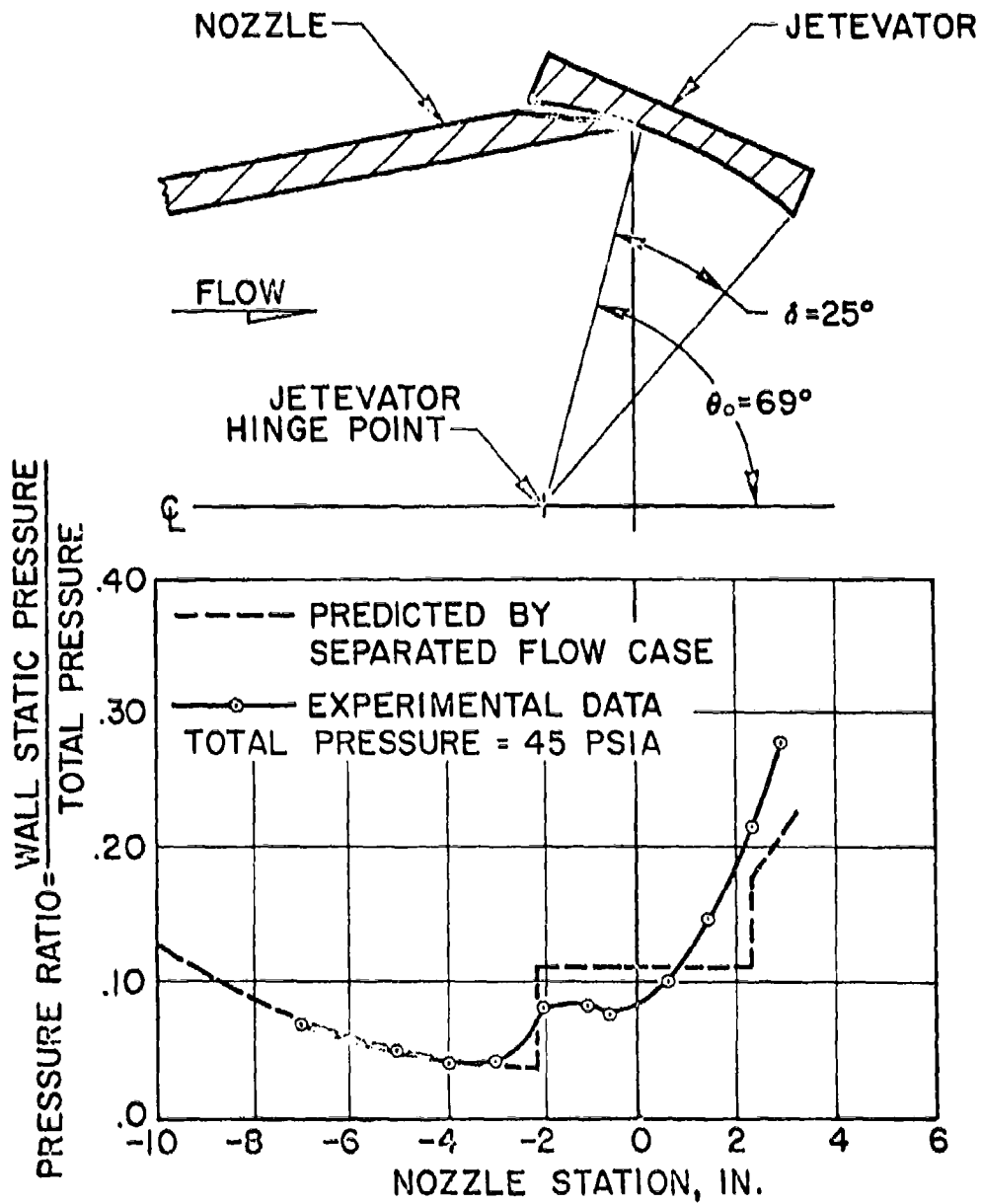
CONFIDENTIAL/DECLASSIFIED

Fig. 8 Comparison of Predicted Pressure Distribution with Experimental Data

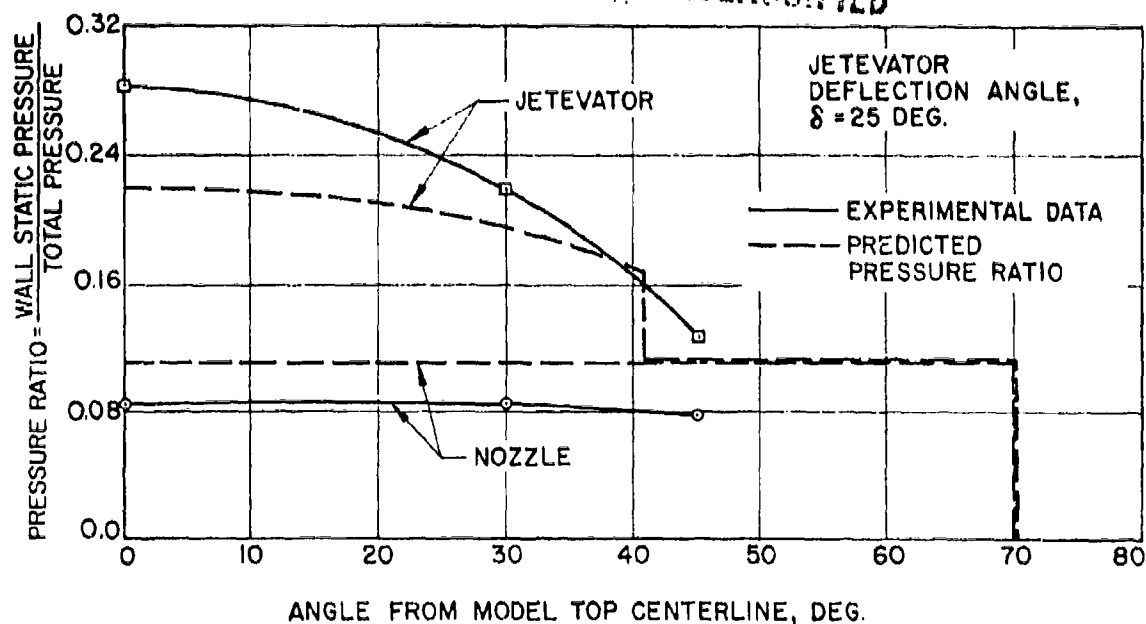


Fig. 9 Radial Distribution of Peak Pressures for Separated Flow Case

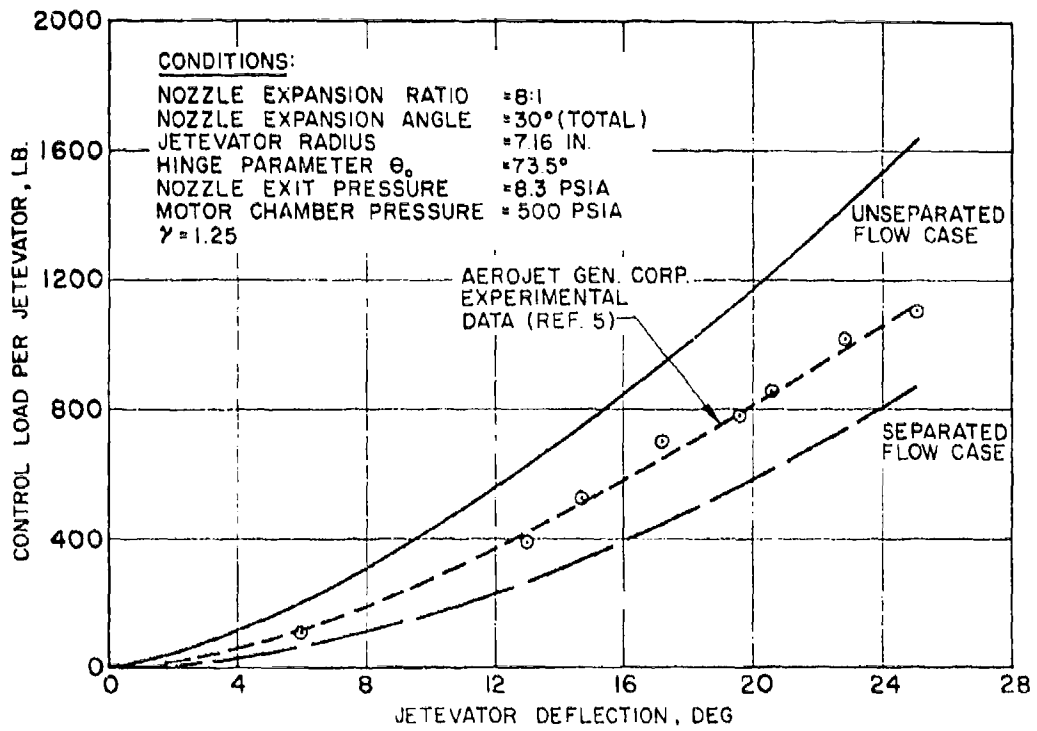


Fig. 10 Comparison of Loads Predicted by Analytical Study to Experimental Data

~~CONFIDENTIAL~~
~~CLASSIFIED~~

of the jetevator hinge point with respect to the nozzle exit plane. Since the location of the hinge point determines the angle θ_0 (see Fig. 5) and the initial flow turning angle from the nozzle to jetevator, it was expected that the separation characteristics in the nozzle and the pressure distribution over the jetevator would be affected by a change in hinge point position. In the tests, the hinge point location was varied to give a 7° change in θ_0 and the results are shown in Fig. 11. As the flow-turning angle increased (representing a decrease in θ_0), the point of separation moved upstream in the nozzle and the pressures over the aft surface of the jetevator increased.

Since the phenomenon of flow separation in the nozzle is a result of an adverse pressure gradient due to the initial flow turning angle at the juncture of the nozzle and jetevator, an investigation was made using the gap between the nozzle and jetevator as a means of boundary layer control. By opening the gap, and thus venting the high pressure region to the low back pressure, it was found that the flow boundary over the jetevator was changed causing greater compression which in turn resulted in higher pressures over the aft three-fourths of the jetevator. Figure 12 presents the center-line pressure distribution for a minimum nozzle-to-jetevator gap clearance (indicated as "0" on the figure) and a gap of 0.20 in. Similar increases in pressure were recorded at stations measured 30° , 45° , and 60° radially from the center-line. Later tests run on similar configurations showed the optimum gap to be in the order of 0.30 in. These results have not yet been confirmed in rocket motor firings due to the serious problem of the hot gases which blow back through the gap. The gap effects are particularly interesting inasmuch as rocket firing experience has indicated that serious difficulties can be encountered with spalling metal essentially welding the jetevators to the nozzle if small gaps are maintained. On the other hand, if shielding shrouds have to be provided to deflect blowby gas, a weight penalty is incurred.

The effect of nozzle trailing edge thickness on the pressure distribution was also investigated. A comparison of the pressure data for a nozzle with a sharp trailing edge at a jetevator deflection of 25° (see

CONFIDENTIAL/CLASSIFIED
~~CONFIDENTIAL/CLASSIFIED~~

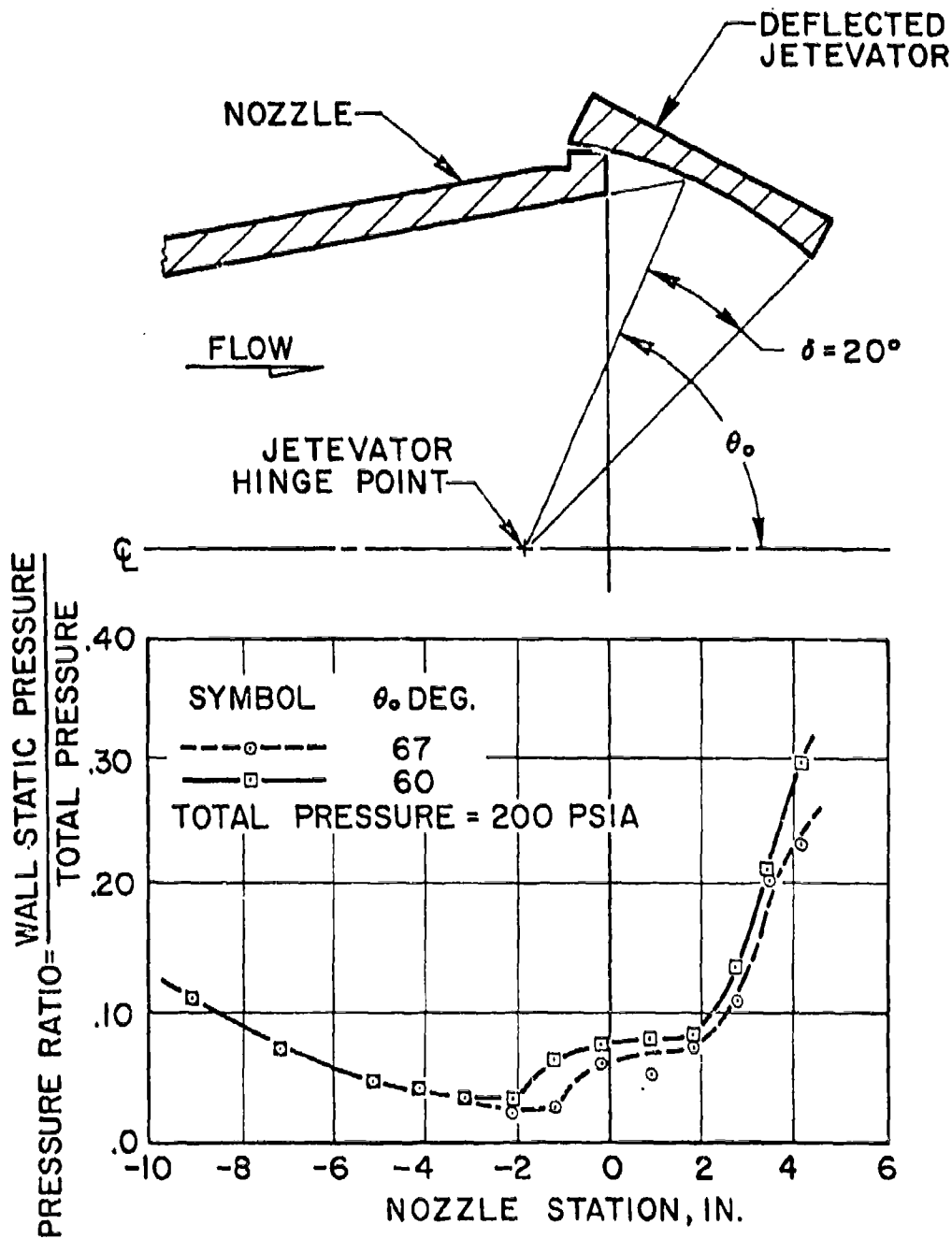


Fig. 11 Effect of Jetelevator Hinge Location on the Pressure Distribution along Nozzle and Jetelevator Centerline

CONFIDENTIAL

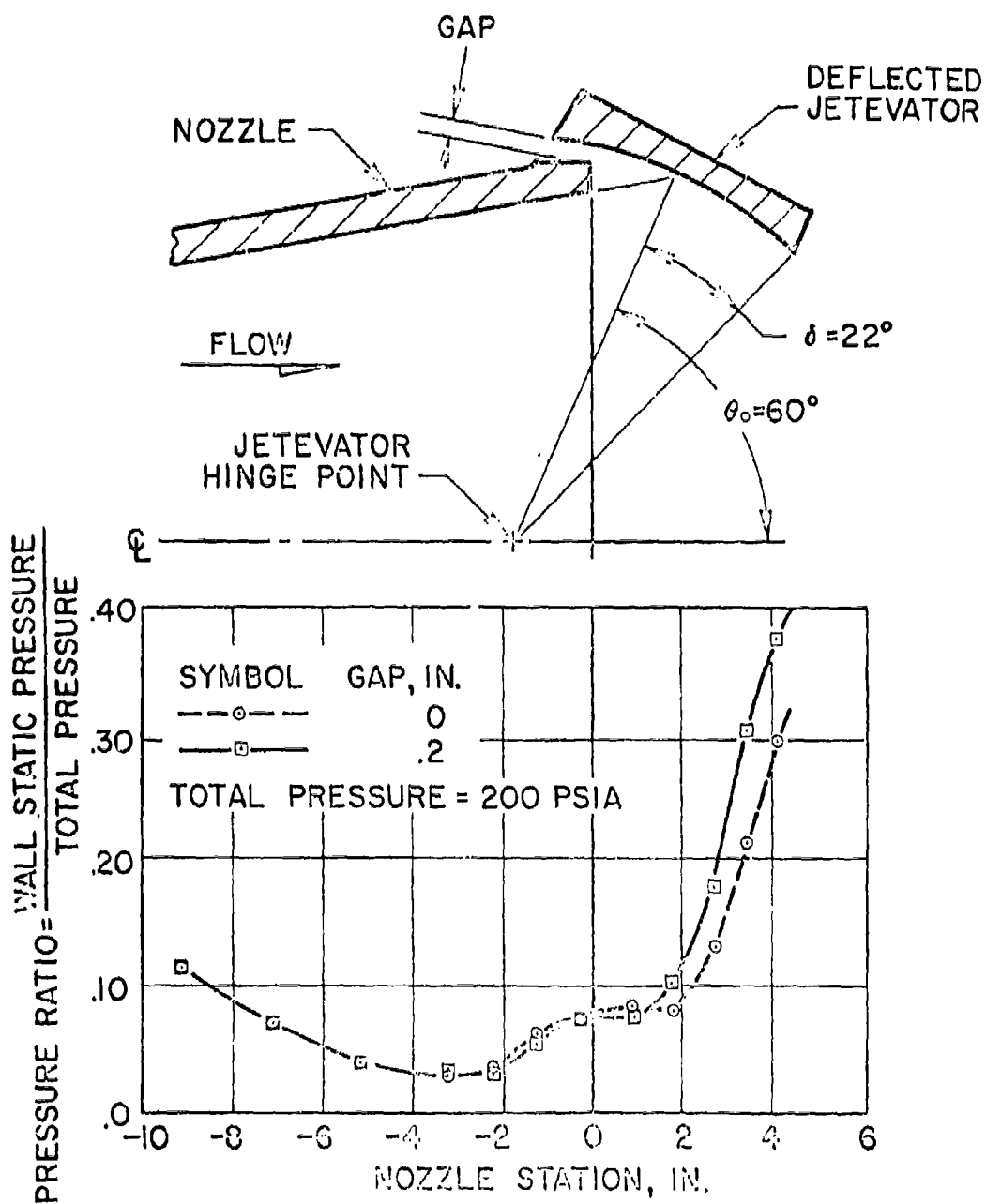


Fig. 12 Effect of Gap on Pressure Distribution along Nozzle and Jetelevator Centerline

CONFIDENTIAL

~~CONFIDENTIAL~~

LM6D-2630

Fig. 8) to the one with a thick trailing edge for the case of "0" gap clearance (see Fig. 12) shows:

1. Separation occurs at a more forward point in the nozzle.
2. The pressure rise occurs over a more forward portion of the jetevator.
3. A lower peak pressure is obtained for the case of the sharp trailing edge.

Sufficient data on the effect of nozzle trailing edge thickness are not available. The data to date indicate however, that it is desirable to design the nozzle trailing edge as thin as can be tolerated by the ability of the material to withstand heating. In fact, in several rocket firings excessive nozzle trailing edge thickness is considered to have contributed to serious load reversals at small jetevator deflection angles and nonlinearity of control load as a function of jetevator angle.

~~CONFIDENTIAL~~

CONCLUSIONS

The analysis presented has proved to be very useful not only in preliminary design investigations of jetevators but also in studies of the stability and control of missiles employing jetevator control systems. It is believed that the most pertinent parameters have been included; however, it is recognized that a number of assumptions related primarily to the problems of real gas flows have been made. The most troublesome areas, of course, are the formulation of an analytical expression for the pressure distribution on the jetevator and the specification of the flow separation boundaries and their effect upon the pressure distribution. Conceivably, further examination of second order expressions for the pressure distribution (see Eq. 4) and a more detailed study of the effects of pressure gradient upon boundary layer separation will improve the accuracy of analytical computations. However, only a limited number of jetevator tests have been made to date, and much of the information required to more accurately formulate the analytical framework will probably come in future tests of the devices.

~~CONFIDENTIAL~~

~~CONFIDENTIAL~~
~~CONFIDENTIAL~~

LMSD-1630

REFERENCES

1. A. Leone, "Survey of Methods for Deflecting Exhaust in Missile Control". U. S. Naval Air Rocket Test Station Report No. 60, September 1955. Confidential.
2. W. A. Fiedler, "Thrust Direction Control by Jetvator", Progress Summary Report No. 15, USNAMTC, Point Mugu, Calif., May 1956.
3. Roy H. Lange, "Present Status of Information Relative to the Prediction of Shock-Induced Boundary-Layer Separation". NACA TN 3065, February 1954.
4. Eli Reshofho and Maurice Tucker, "Effect of a Discontinuity on Turbulent Boundary-Layer Thickness Parameters with Application to Shock-Induced Separation", NACA TN 3454, May 1955.
5. R. A. Nilson, "Final Test Report-XM-36 Thrust Alignment Test". Aerojet-General Corporation Test No. D-232-SA-1, September 1957. Confidential.